ELSEVIER

International Journal of Refrigeration 26 (2003) 601–613

REVUE INTERNATIONALE DU FROID
INTERNATIONAL JOURNAL OF
refrigeration

www.elsevier.com/locate/ijrefrig

Modelling and optimisation of wire-and-tube condenser

P.K. Bansal*,[1], T.C. Chin

Department of Mechanical Engineering, The University of Auckland, Private 92019, Auckland, New Zealand

Received 19 November 2001; received in revised form 4 July 2002; accepted 4 July 2002

Abstract

This paper presents the modelling and experimental results of wire-and-tube condensers that are commonly used in vapour compression cycle based domestic refrigerators. A condenser was experimentally tested in a real refrigerator for some operating conditions. A simulation model was developed using the finite element and variable conductance approach, along with a combination of thermodynamic correlations. The condenser capacity per unit weight was optimised using a variety of wire and tube pitches and diameters. An *optimisation factor*, f_o was defined as ratio of the condenser capacity per unit weight of the optimised design and the present design. The application of this factor led to an improved design with 3% gain in capacity and 6% reduced condenser weight.

Keywords: Condenser; Tube; Wire; Domestic refrigerator; Heat transfer; Optimization; Modelling

Modélisation et optimisation d'un condenseur à tubes et fils

Mots clés : Condenseur ; Tube ; Fil ; Réfrigérateur domestique ; Transfert de chaleur ; Optimisation ; Modélisation

1. Introduction

Currently, refrigeration research focuses on improving energy efficiency, reducing manufacturing cost and introducing innovative designs of heat exchangers (compact, functional, user-friendly). A well-designed condenser will not only improve the energy efficiency, but will also reduce the space and material for a specific cooling capacity. One of the commonly used condensers in domestic refrigerators is the wire-and-tube condenser. The wire-and-tube condenser (denoted as W&T hereon) is predominantly a natural convection heat exchanger. It consists of a single copper tube and solid steel wires that serve as extended surfaces. The tube which carries the refrigerant, is bent into a single-passage serpentine shape with wires symmetrically spot-welded to both sides in a direction normal to the tubes as shown in Fig. 1a. It had been used and widely studied since 1960s. Hoke et al. [1] and Lee and Lee [2] developed the air-side empirical heat transfer correlations for forced-convection W&T condensers while Tagliafico and Tanda [3] for natural-convection type condensers.

It is envisaged that a computer model would act as a convenience tool for analysing the performance of the condenser for different design parameters such as tube diameter and mass flow rate, and reducing the cost of testing and prototype manufacturing of new or modified condensers. Heat exchanger models had been developed by numerous researchers, including Admiraal and Bullard [4], Bansal et al. [5,6], Judge and Radermacher [7], Pettit et al. [8] and Reeves et al. [9]. These models were based on refrigerant flow inside the tube and cross-flow or counter-flow forced convective heat transfer on the outside. However, the W&T condenser is a natural draft

* Corresponding author. Fax: +64-9-373-7479.
E-mail address: p.bansal@auckland.ac.nz (P.K. Bansal).
[1] Member of Commission E1 of IIR.

0140-7007/03/$35.00
PII: S0140-7007(02)00044-0

Nomenclature

A	area (m^2)
c_p	constant pressure specific heat (J kg^{-1} K^{-1})
d	diameter (m)
f	friction factor (–)
f_c	condenser capacity factor (–)
f_o	optimisation factor (–)
f_w	condenser weight factor (–)
g	acceleration due to gravity (m s^{-2})
G	flow rate per unit area or mass flux (kg m^{-2} s^{-1})
h	heat transfer coefficient (W m^{-2} K^{-1})
h	refrigerant enthalpy (kJ kg^{-1})
H	heat exchanger height (m)
h_{fg}	heat of vaporisation (kJ kg^{-1})
j_g^*	mass velocity (–)
k	thermal conductivity (W m^{-1} K^{-1})
l	length (m)
m	fin property parameter (–)
$\dot{m}$	mass flow rate (kg s^{-1})
Nu	Nusselt number (–)
p	pitch (m)
P	Pressure (kPa)
Pr	Prandtl number (–)
$\dot{Q}$	heat flow rate (W)
$\dot{q}$	heat flux (W m^{-2})
R	thermal resistance (K/W)
Ra	Rayleigh number (–)
Re	Reynolds number (–)
t	thickness (m)
T	temperature (K)
U	unit conductance (W m^{-2} K^{-1})
W	weight (kg)
x	Refrigerant quality (–)
X_{tt}	Martinelli parameter (–)
Δz	Elemental length (m)

Greek letters

θ	angle of inclination of a tube (degree)
π	phie, $\pi = 3.1416$
α	Void fraction (–)
β	thermal expansion coefficient (K^{-1})
ε	thermal emittance (–)
ν	efficiency (–)
μ	dynamic viscosity (kg m^{-1} s^{-1})
ν	Kinematic viscosity ($m^2.s^{-1}$)
ρ	Density (kg m^{-3})
σ	Stefan–Bolzmann constant, $\sigma = 5.67\times10^{-8}$ (W K^{-4} m^{-2})

Subscripts

a	air/accelerational
app	apparent
c	convective
ele	elemental
ex	heat exchanger
eq	equivalent
f	frictional
g	gravitational
i	inside, inlet
ix	inside cross section
l	liquid phase
o	outside, outlet
opt	optimisation
pl	plate
r	radiative
ref	refrigerant
s	surface
sat	saturation
t	tube
tot	total
v	vapor/gas phase
w	wire
∞	free stream/ambient

type heat exchanger with relatively different tube geometry and flow direction, and hence, a distinct model needs to be developed for its performance assessment. The aim of this paper is to present the development and application of such a model for design and optimisation purposes of the W&T condensers in domestic refrigerators. The model was developed using the finite element and variable conductance approach, along with a combination of thermodynamic correlations. It was written in FORTRAN 90 programming language. For refrigerant property data, REFPROP [10] software was implemented in the model. It is a computer database used in refrigeration industry to evaluate the thermodynamic and transport properties of a wide range of refrigerants and refrigerant blends.

2. Modelling of the condensers

The schematics and elemental unit of the condenser are shown in Fig. 1. The condenser model was developed using finite element and variable conductance approach (shown in Fig. 2) to model the performance of the W&T condenser. The rate of heat transfer from an element of tube length, Δz (see Fig. 2) can be expressed as

$$\dot{Q}_{ele} = UA_{ele}.(T_{ref} - T_{\infty})_{ele.} \quad (1)$$

The variable conductance, UA_{ele} applied to each element is expressed as

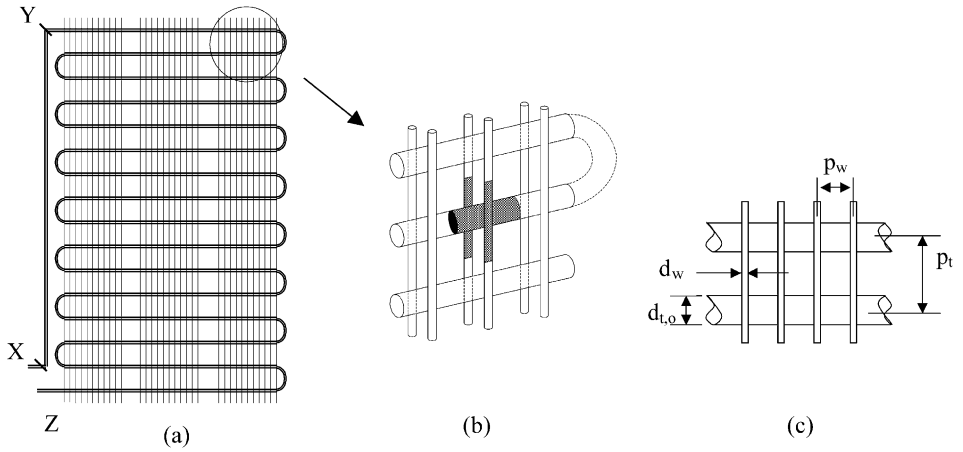

Fig. 1. (a). Schematics of a wire-and-tube condenser, (b) elemental unit of the condenser, and (c) parameters of the wire-and-tube condenser.

$$\frac{1}{UA_{ele}} = R_i + R_t + R_o = \left(\frac{1}{h_i A_i} + \frac{\ln(r_o/r_i)}{2\pi.k.\Delta z} + \frac{1}{h_o A_o}\right)_{ele} = R_{W\&T} \quad (2)$$

It is primarily a function of the inner heat transfer, radial heat conduction (in the tube) and outer heat transfer resistances. The elemental tube length is equal to the pitch of wire, $\Delta z = p_w$ (see Figs. 1c and 2) and the elemental outer area of heat transfer, A_o is given as

$$A_o = A_t + A_w = \pi.d_{t,o}.p_w + 2.\pi.d_w.p_t \quad (3)$$

The design parameters for the current condenser are given in Table 1. The computation of the convective heat transfer requires the knowledge of the fin efficiency of the wire, η_w which depends on the temperature distribution along the wire due to conduction and convection. Assuming the heat transfer coefficient to be constant along the elemental segment of the wire, the one-dimensional fin efficiency, η_w is expressed as

$$\eta_w = \frac{\left[\tanh(\frac{mp_t}{2})\right]}{\left[\frac{mp_t}{2}\right]} \text{where } m = \sqrt{\frac{4h_w}{k_w d_w}} \quad (4)$$

Initially, the convective heat transfer coefficient of the wire, h_w is guessed in a way that Eq. (4) yields the fin efficiency (η_w) of about 0.9 to start the iterations. By definition, the fin efficiency is the ratio of temperature difference between the wire and the ambient, and the tube and ambient as given by:

$$\eta_w = \frac{(T_w - T_\infty)}{(T_{t,o} - T_\infty)} \text{ or } T_w = \eta_w.(T_{t,o} - T_\infty) + T_\infty \quad (5)$$

Initially, the outer tube temperature $T_{t,o}$, is assumed to be 0.5 °C lower than the refrigerant temperature. This value is iterated after the elemental heat transfer has been computed. The calculation of the convective and radiative heat transfer requires the evaluation of the

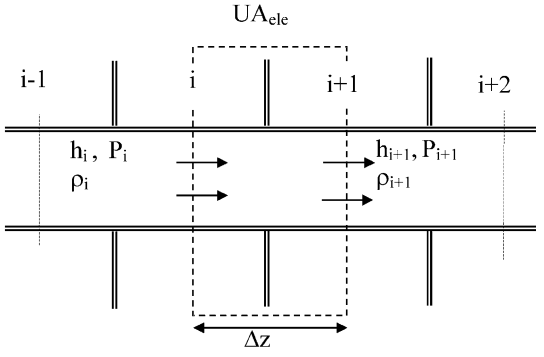

Fig. 2. Finite element and variable conductance model.

Table 1
Design parameters and geometrical data of current wire-and-tube condenser

Tubing material	Copper tubing powder-coated with white
Tube outer diameter, $d_{t,o}$ (mm)	4.5
Tube pitch, p_t (mm)	45
Total tube length (m)	18.10
Inner flow area (m^2)	9.62×10^{-6}
Inner wetted area (m^2)	0.1990
Outer heat transfer area (m^2)	3.248
Number of rows	26
Wire diameter, d_{wi} (mm)	1
Wire pitch, p_{wi} (mm)	4.8
Number of wires (pairs)	81

mean surface temperature of the heat exchanger, T_{ex}. This can be expressed as a function of the surface temperature of the tubes, $T_{t,o}$ and the mean surface temperature of the wires, T_w as:

$$T_{ex} = \frac{(A_t T_{t,o} + A_w T_w)}{A_o} \tag{6}$$

Substituting Eqs. (3) and (5) into (6), T_{ex} can be written as:

$$T_{ex} = \frac{(T_{t,o} + GP.\eta_w.(T_{t,o} - T_\infty) + GP.T_\infty)}{(1 + GP)} \tag{7}$$

where GP, the geometric parameter is expressed as

$$GP = 2.\left(\frac{p_t}{d_{t,o}}\right).\left(\frac{d_w}{p_w}\right) \tag{8}$$

3. Outer heat transfer coefficients

The outer heat transfer coefficient, ho comprises the convective and radiative heat transfers as:

$$h_o = h_c + h_r \tag{9}$$

The radiative heat transfer coefficient is given by:

$$h_r = \varepsilon_{app}.\sigma.\frac{(T_{ex}^4 - T_\infty^4)}{(T_{ex} - T_\infty)} \tag{10}$$

where σ is the Stefan–Boltzmann constant, 5.67×10^{-8} W K^4 m^2 and ε_{app} is the apparent emissivity, a parameter which identifies the radiation behaviour of the heat exchanger. It is a complex function of thermal emittance of the heat transfer surface, ε (0.91 for the white enamel surface) and the diameter and pitch of the wire and tube. In general, the higher the thermal emittance, the less sensitive (to the tube and wire parameters) the apparent emisstivity, ε_{app} becomes. A fixed value of $\varepsilon_{app} = 0.88$ is used to simplify the analysis while ensuring good agreement between the experimental and modelling results.

The computation of the convective heat transfer involves two sections of the heat exchanger, namely the X–Y and Y–Z sections (see Fig. 1a). The convective heat transfer coefficients for the vertical section (X–Y) was computed using McAdam correlation [11] given as:

$$h_c = 0.27\left(\frac{\Delta T}{d_o}\right)^{0.25} \tag{11}$$

For the Y–Z section, which is main frame of the W&T condenser, the convective heat transfer was computed using Tagliafico and Tanda [3] correlation. This semi-empirical correlation, given by Eq. (12), was developed using the experimental data from 42 low-emittance wire-and-tube exchangers with various geometrical characteristics to yield an average convective heat transfer coefficient for the whole heat exchanger

$$h_c = \frac{\mathrm{Nu} \times k_a}{H} \tag{12}$$

where

$$\mathrm{Nu} = 0.66.\left(\frac{\mathrm{Ra}.H}{d_{t,o}}\right)^{0.25} .\left\{1 - \left[1 - 0.45\left(\frac{d_{t,o}}{H}\right)^{0.25}\right].\exp\left(-\frac{s_w}{\varphi}\right)\right\} \tag{12a}$$

$$\mathrm{Ra} = \left(\frac{\beta\rho^2 c_p}{\mu k}\right)_a g.(T_{t,o} - T_\infty).H^3 \tag{12b}$$

$$\varphi = (28.2/H)^{0.4} s_w^{0.9} s_t^{-1.0} + (28.2/H)^{0.8}.\left[264/(T_{t,o} - T_\infty)\right]^{0.5} s_w^{-1.5} s_t^{-0.5} \tag{12c}$$

$$s_t = (p_t - d_t)/d_t;\ \ s_w = (p_w - d_w)/d_w \tag{12d}$$

The outer heat transfer coefficient, h_o, is compared with the initial guessed value of the wire heat transfer coefficient, h_w. If the difference is larger than 0.01 W m^2 K, set $h_o = h_w$ in Eq. (2) and computations are repeated from Eqs. (4)–(12) until convergence was achieved. This iteration loop is called the *outer heat transfer coefficient loop* (h_o loop) as shown in Fig. 3.

4. Internal convective heat transfer coefficients

During film condensation inside a tube, a variety of flow patterns can exist. These include bubbly, slug, wavy, stratified and annular flows [11]. Generally, different heat transfer models are used to calculate the heat transfer coefficient depending on whether vapor shear or gravitational forces are more important. The transition from one flow pattern to another must be predicted to enable the selection of correlations. Breber et al. [12] proposed a simple method of predicting flow pattern transitions that depend on the dimensionless **mass velocity**, j_g^*, defined as:

$$j_g^* = \frac{xG}{[gd_{t,i}\rho_g(\rho_l - \rho_v)]^{1/2}} \tag{13a}$$

and the Lockhart–Martinelli parameter:

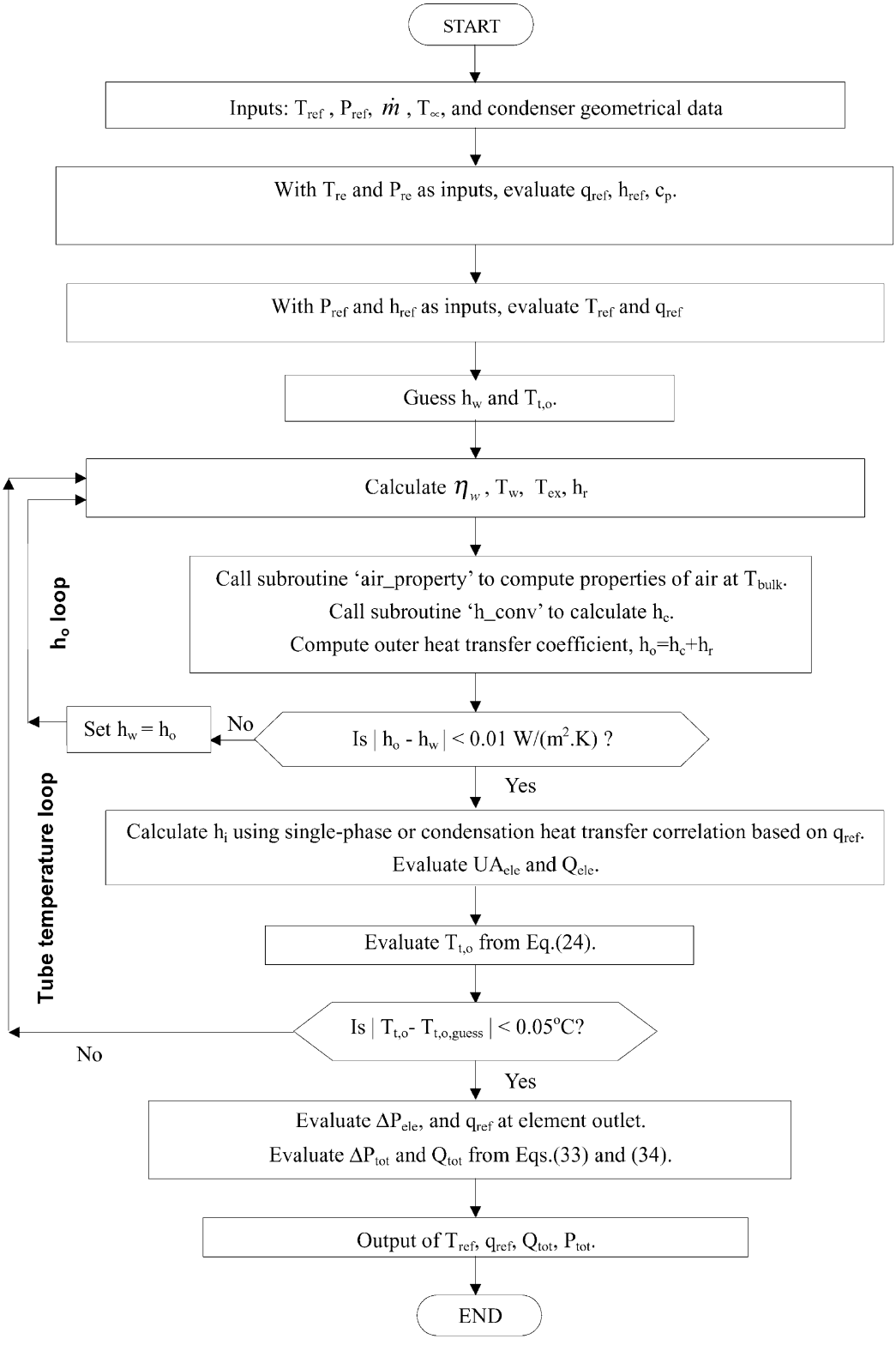

Fig. 3. Flowchart for the computer model of the wire-and-tube condenser.

$$X_{tt} = \left(\frac{1-x^*}{x^*}\right)^{0.875}\left(\frac{\mu_l}{\mu_v}\right)^{0.125}\left(\frac{\rho_v}{\rho_l}\right)^{0.5} \quad (13b)$$

The flow pattern criteria were as follows:

$$\begin{aligned} &j_g^* > 1.5,\ X_{tt} < 1.0 \text{ mist andannular}\\ &j_g^* < 0.5,\ X_{tt} < 1.0 \text{ wave andstratified}\\ &j_g^* < 0.5,\ X_{tt} > 1.5 \text{ slug}\\ &j_g^* > 1.5,\ X_{tt} < 1.5 \text{ bubble} \end{aligned} \quad (14)$$

Slug and bubbly flows scarcely occur during the condensation process and were not considered.

4.1. Correlation for annular flow in horizontal tubes

Cavillini and Zecchin correlation [13] was used to compute the condensation heat transfer coefficient for annular flow. It had been verified of its wider application for a variety of refrigerants or refrigerant mixtures in the literature [14–16]. It uses an equivalent Reynolds Number Re_{eq} to replace the normal Reynolds number used in common Nusselt correlations as shown below:

$$Nu_{tp} = \frac{h_{tp}d}{k_l} = 0.05\ Re_{eq}^{0.8} Pr_l^{0.33} \quad (15a)$$

Re_{eq} is computed using the liquid and vapour Reynolds number, Re_l and Re_v given by:

$$Re_{eq} = Re_v\left(\frac{\mu_v}{\mu_l}\right)\left(\frac{\rho_l}{\rho_v}\right)^{0.5} + Re_l \quad (16a)$$

$$\text{where } Re_v = \frac{G.x.d}{\mu_v} \text{and } Re_l = \frac{G.(1-x).d}{\mu_l} \quad (17)$$

4.2. Correlation for stratified flow in horizontal tubes

The average heat transfer coefficient for stratified flow over the entire perimeter may be expressed by a modified Nusselt number [17] as:

$$h_m = \Omega\cdot\left[\frac{(\rho_l(\rho_l-\rho_v).g.h_{fg}\cdot k_l^3)}{(d_{t,i}.\mu_l.\Delta T)}\right]^{0.25} \quad (18)$$

where the coefficient Ω depends on the fraction of the tube that is stratified. Jaster and Kosky [18] had shown that Ω is related to the void fraction of the vapour, α_g as:

$$\Omega = 0.728\alpha_g^{3/4} \text{ where } \alpha_g = \frac{1}{1+[(1-x)\ /\times]\cdot(\rho_v/\rho_l)^{2/3}} \quad (19)$$

4.3. Condensation heat transfer for downward flow in vertical tube

There are very limited correlations developed for flow in vertical tubes. The downward flow of the refrigerant in a vertical tube is stratified (low-shear region) when the mass velocity $j_g^* \leqslant 0.5$. The following condensation equations were used depending on the Reynolds numbers [19]:

$$\frac{h}{k}\left[\frac{\mu^2}{\rho_l(\rho_l-\rho_v)g}\right]^{1/3} = 1.1\times Re^{-1/3} \text{ for } Re \leqslant 40 \quad (20)$$

For $Re > 40$, the larger of the two coefficients, calculated from the rippled laminar or the turbulent equations, were used

$$\frac{h}{k}\left[\frac{\mu^2}{\rho_l(\rho_l-\rho_v)g}\right]^{1/3} = 0.8 \times Re^{-0.22}\text{Rippled laminar} \quad (21)$$

$$\frac{h}{k}\left[\frac{\mu^2}{\rho_l(\rho_l-\rho_v)g}\right]^{1/3} = 0.023\times Re^{1/4}Pr^{0.5} \quad \text{Turbulence} \quad (22)$$

4.4. Condensation heat transfer for upward flow in vertical tube

For upward vapour flow with a returning condensate, the vapour velocities are generally low to avoid flooding. The interfacial shear retards the drainage of the condensate. As a result, the condensate film thickens and the heat transfer coefficient decreases. The average coefficient is given by Mueller [19]:

$$\frac{\overline{h}}{k}\left[\frac{\mu^2}{\rho_l(\rho_l-\rho_v)g}\right]^{1/3} = 1.47\times Re^{-1/3} \quad (23)$$

Having found the inner and outer heat transfer coefficients, the elemental heat transfer, $\dot{Q}_{ele}$ was computed from Eqs. (1) and (2). As the heat transfer from the refrigerant to the ambient must be equal to the heat transfer from the refrigerant to the tube outer surface (in the steady state), the outer tube temperature, $T_{t,o}$ can be obtained from the following

$$T_{t,o} = T_{ref} - \dot{Q}_{ele}\cdot\left(\frac{1}{h_i A_i} + \frac{\ln(r_o/r_i)}{2\pi k l}\right)_{ele} \quad (24)$$

This value is then compared against the initial value of $T_{t,o}$. If the error is larger than 0.05 °C, a new $T_{t,o}$ is substituted into Eq. (7) and the computations are repeated until convergence is achieved. This yields the actual heat transfer. This iteration loop is called the 'tube temperature loop', and is shown in Fig. 3. The enthalpy of the refrigerant at the outlet of an element can then be given by:

$$h_{\text{out, ele}} = \frac{\dot{Q}_{\text{ele}}}{\dot{m}} + h_{\text{in, ele}} \tag{25}$$

5. Pressure loss correlations

The total pressure loss across the condenser is the summation of the frictional, accelerational, gravitational and local pressure drops (such as bend loss). For single-phase flow, the friction loss is given by [11]:

$$\left(\frac{\mathrm{d}P}{\mathrm{d}z}\right) = -f\frac{1}{d_{t,i}}\frac{\dot{m}^2}{2\rho} \text{ where } f = (0.79\ln \mathrm{Re_d} - 1.64)^{-2} \tag{26}$$

The two-phase frictional pressure drop generally constitutes the largest part of the total pressure drop, although its calculation can only rely extensively upon empirical methods. It involves not only the transfer of momentum or shear stress between the fluid and the wall, but also the transfer of momentum between the individual phases. For the calculation of the frictional pressure drop, it is advantageous to define several parameters that are suitable for the description of the two-phase frictional pressure drop and quality. In particular, the frictional pressure drop is reduced to the pressure drop of the single-phase flow by using the definitions developed by Lockhart and Martinelli [20] as given below:

$$\left(\frac{\mathrm{d}P}{\mathrm{d}z}\right)_f = \phi_l^2\left(\frac{\mathrm{d}P}{\mathrm{d}z}\right)_l \text{ where } \left(\frac{\mathrm{d}P}{\mathrm{d}z}\right)_l = -f_l\frac{1}{\mathrm{d}}\frac{\dot{m}_l^2}{2\rho_l} \tag{27}$$

The liquid-phase mass flow and friction factors are:

$$\dot{m}_l = \dot{m}(1-x) \text{ and } f_l = 0.0316\ \mathrm{Re}_l^{-0.25} \text{ for } 2400 < \mathrm{Re} < 3\times 10^6 \tag{28}$$

The liquid phase multiplier, ϕ_l is a correction factor for the frictional pressure drop of the single phase and can be defined as a function of the Martinelli parameter X_{tt} [21]as:

$$\phi_l^2 = 1 + \frac{8}{X_{tt}} + \frac{1}{X_{tt}^2} \tag{29}$$

The ***gravitational*** pressure drop is given by the following equation where ρ_{av} is computed using REFPROP [10] software:

$$\left(\frac{\mathrm{d}p}{\mathrm{d}z}\right)_g = [\varepsilon\rho_v + (1-\varepsilon)\rho_l].g.\sin\theta = \rho_{av}g.\sin\theta \tag{30}$$

The pressure drop due to ***acceleration*** results from the change in momentum of the two phases during the condensation process where pressure gain and heat loss take place. It can be expressed in terms of the elemental inlet and outlet density as:

$$\Delta P_a = \mathrm{G}^2\left[\frac{1}{\rho_o} - \frac{1}{\rho_i}\right] \tag{31}$$

$$\Delta P_{\text{ele}} = P_{\text{out, ele}} - P_{\text{in, ele}} = \Delta P_f + \Delta P_g + \Delta P_a \tag{32}$$

As the outlet density, ρ_o is not known, initially, set $\Delta P_a = 0$ and the outlet elemental pressure, $P_{\text{out,ele}}$ is evaluated. Subsequently ρ_o can be found using REFPROP built-in subroutine, as being a function of $P_{\text{out,ele}}$ and $h_{\text{o,ele}}$. The whole process is iterated until ρ_o converges.

The total pressure loss and heat transfer rate are simply the sum of all elemental pressure losses and heat transfer (that are updated after each iteration) as:

$$\Delta P_{\text{tot}} = \sum \Delta P_{\text{ele}} \tag{33}$$

$$\dot{Q}_{\text{tot}} = \sum \dot{Q}_{\text{ele}} \tag{34}$$

The computation process is repeated for subsequent elements where the inlet conditions of the current element is equal to the outlet conditions of the previous element, namely:

$$\left(T_i, P_i, \rho_i, q_{\text{ref,i}}, h_i\right)_i = \left(T_o, P_o, \rho_o, q_{\text{ref,o}}, h_o\right)_{i-1} \tag{35}$$

This yields the computation of the condenser capacity, pressure drop and other performance characteristics of the condenser as discussed in the following sections.

6. Experimental validation of the results

To validate the model, experiments were conducted on a wire-and-tube condenser using a real refrigerator. The details of the experimental devices and procedures are summarised in Chin [21]. The condenser was tested on a two-door vapour compression cycle based domestic

refrigerator-freezer (model E406B). The capacity of the Provision Compartment (PC) and the Freezer Compartment (FC) was respectively 271 and 133 l. The fridge had a reciprocating compressor (model Embraco FGS90HAW), a defrost heater of 350 W, an egg-crate type evaporator [6], a non-adiabatic capillary tube along with a wire-and-tube condenser. Closed-door experiments were carried out on the refrigerator in an environmental chamber, which was maintained at 20 or 25 °C (±0.5 °C) and at 55% relative humidity (±5%) for all the tests. Measurements of refrigerant temperature, pressure and mass flow rate, and power consumption by the refrigerator were taken during the experiments.

The modeling results were compared with the experimental results for different saturation temperature conditions where the refrigerant was fully condensed at the condenser outlet. The comparative results of the condenser capacity and pressure loss are shown in Figs. 4 and 5 respectively. In term of the condenser capacity, the modelled results agree with the experimental results to within ±10%. The majority of the modelled capacities under-predict the experimental values. The modelled results for the pressure loss agree with the experimental results to within ±15%. Modeled pressure drops tend to be higher than the experimental data. These disagreements could be attributed to a number of factors as follows. As the state of the refrigerant is determined by the measured temperatures and pressures, a minor error in the measurement may lead to the refrigerant condition being taken as fully condensed, while in fact, the refrigerant may still be in the two-phase state. The capacity for these two conditions could differ considerably. This condition may specifically be relevant to situations where the degree of sub-cooling is less than 0.5 °C. The model can be further improved by calculating the apparent emissivity instead of using a constant value of 0.88 to accommodate its variation with tube and wire parameters.

7. Heat transfer characteristics

Radiative and convective are the two heat transfer mechanisms at the outer surface of the condenser. These with the overall heat transfer coefficient were modelled for $G = 115\ \mathrm{kg^{-1}\ s\ m^2}$, $T_{sat} = 40\ ^\circ\mathrm{C}$ and $T_\infty = 20\ ^\circ\mathrm{C}$ as shown in Fig. 6 where the x-axis represents the position along the condenser as a fraction of the total tube length. The overall heat transfer coefficient, U_o was computed using the elemental UA values and outer transfer area given by:

$$U_o = UA_{ele}/A_{o,ele} \tag{36}$$

The notations used in Figs. 6 and 7 are described in Table 2. At the superheated unfinned region (A), the radiation heat transfer dominates the heat transfer. Moving along the condenser, the fluid flows through the finned horizontal section (region B) of the condenser. The convective heat transfer coefficient, h_c increases significantly [to $\sim$10 W/(m^2 K)] as the wire fins provide additional heat transfer area. Region C is the condensation region. The inner heat transfer coefficient increases rapidly, resulting in the increase of U_o from region B to C. The convective heat transfer coefficient, h_c remains almost constant at 9.8 W ($\mathrm{m^{-2}\ K^{-1}}$). The sudden drop of the coefficients (to about 6 W $\mathrm{m^{-2}\ K^{-1}}$) along the h_c curve, corresponds to the coefficients at the unfinned section of the W&T condenser. In the sub-cooled region (D), the refrigerant temperature drops considerably. Thus, h_c drops accordingly.

In general, h_c depends on the both the geometry of the heat transfer area and the temperature. The overall heat transfer coefficient, U_o is used to compute the heat transfer using the temperature difference between the refrigerant and the ambient temperature. It exhibits similar pattern with h_c as the convective heat transfer

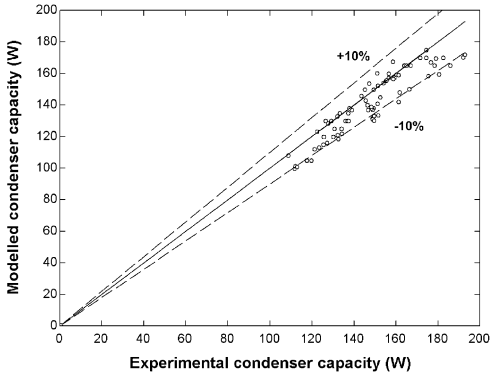

Fig. 4. Comparison of modeling and experimental results for wire-and-tube condenser.

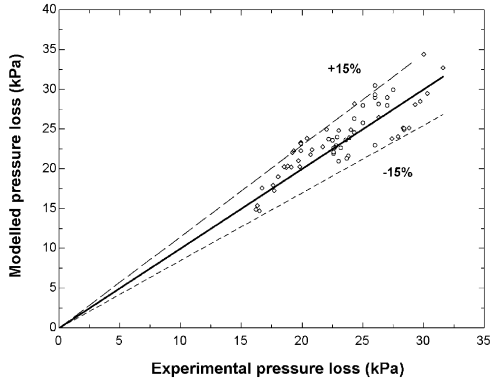

Fig. 5. Comparison of modeling and experimental results for pressure loss across wire-and-tube condenser.

dominates the total heat transfer. The radiation heat transfer coefficient does not change significantly (at about 5.8 W m^{-2} $^{-}$K) across the condenser.

7.1. Heat transfer resistances of W&T condenser

The heat transfer resistance for the W&T condenser consists of the inner, R_i, the outer, R_o and tube heat transfer resistances, $R_{W\&T}$ as shown by Eq. (2). The resistances and temperature profiles were modelled at specific conditions shown in Fig. 7. Outer heat transfer resistance is the most dominant while the tube resistance is negligible. From region A to B, the outer heat transfer resistance reduces significantly as the wires provide additional heat transfer area. As a result, the outer surface temperature decreases, producing a difference of 5 °C between the tube and the refrigerant temperature.

In the condensation region (C), the rapid increase in the inner heat transfer coefficient causes the outer tube surface temperature to rise, resulting in a temperature difference of 0.2 °C between $T_{t,o}$ and T_{ref}. As the condensation proceeds, the proportion of inner resistance reduces slightly, thus, the temperature difference increases gradually (due to refrigerant pressure drop) throughout the condensation process to the maximum of 1.5 °C at the saturated liquid state.

The outer resistance contributes to 83–95% of the total resistance. At the sub-cooled region (D), the temperature difference increases to 2 °C due to increased inner surface heat transfer resistance. As the refrigerant is cooled, the temperature difference reduces due to the proportional increase in the outer heat transfer.

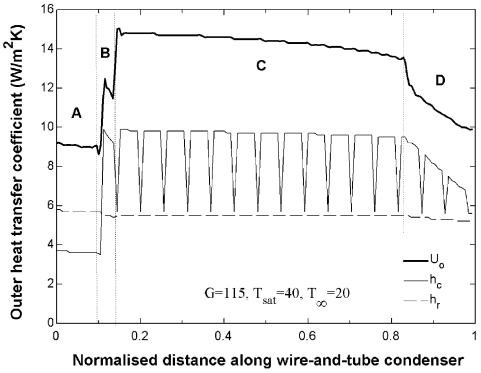

Fig. 6. Variation of the heat transfer coefficients along W&T condenser.

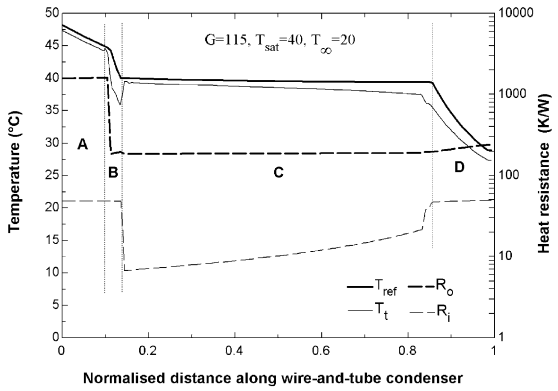

Fig. 7. Variation of the heat transfer resistances and temperature profiles.

8. Modelling of the optimum operating conditions

One of the most significant operating parameters of the condenser is the refrigerant mass flow rate, which determines the pressure loss and compressor work requirement. The condenser capacity and pressure loss were modelled at the condensing temperature of 40 °C with 2 °C superheat at the inlet for different mass flux conditions. Fig. 8 shows that with increasing mass flux, the cooling capacity increases to a maximum of 163 W at 110 kg s^{-1} m^2). When the mass flux is increased further, the capacity drops slightly. Therefore, for larger mass fluxes, a bigger condenser should be used to increase the capacity. If the condensing temperature is increased (from 40 °C) to 50 °C, the condensation heat transfer coefficient increases by around 11–16% for the corresponding mass flux of 80–120 kg m^{-2} s^{-1}. The reverse is true for reduced saturation temperature.

The total pressure loss increases linearly with increasing mass flux. Although the percentage increase in pressure loss was large, the increase in the absolute pressure loss (between 5 and 29 kPa) was relatively insignificant compared to the operating pressure, ranging between 800 and 1000 kPa. During the design of a refrigerant system, it is undesirable to have two-phase refrigerant entering the throttling valve (or the capillary tube). For the maximum mass flow rate, it is desirable that the refrigerant is sub-cooled before it enters the capillary tube. Therefore, the optimum operating conditions for the current condenser, corresponds to a mass flux of 100 kg/(s^{-1} m^{-2}) that yields the capacity of 162 W with 2 °C of sub-cooling and the pressure loss of 16 kPa.

Table 2
Notations used in Figs. 6 and 7

Notations	Physical representation
A	Vapour-phase flow in vertical unfinned section
B	Vapour-phase flow in horizontal finned section
C	Two-phase flow in horizontal finned section
D	Liquid-phase flow in horizontal finned section

The modelled performance of the condenser is shown in Fig. 9 for varying tube diameters at different refrigerant mass flow rates. The pressure loss decreases while the condenser capacity increases with increasing tube outer diameter, $d_{t,o}$. On the other hand, the pressure loss increases with the mass flux. For tube outer diameter, $d_{t,o} < 0.0045$ m, larger mass flux produces smaller capacity and larger pressure loss, while for $d_{t,o} > 0.0045$ m, the reverse is true. Thus, larger mass flow rates are not preferred for $d_{t,o} < 0.0045$ m. Also, the gain in condenser capacity is insignificant ($< 1\%$) when the mass flux is increased above 110 kg m^{-2} s^{-1}.

8.1. Optimisation of the condenser

To find a more economical solution for an improved condenser design, Bansal and Wich [22] introduced a useful parameter called the *optimisation factor*, f_o. This relates the optimum heat exchanger design with the maximum capacity per unit weight. This factor can also be applied to condenser design and is defined as the ratio of the condenser capacity per unit weight of the optimised design ($\dot{Q}_{opt}/w_{opt}$) and the present design ($\frac{\dot{Q}_{100\%}}{w_{100\%}}$) as:

$$f_o = \frac{\dot{Q}_{opt}/w_{opt}}{\dot{Q}_{100\%}/w_{100\%}} \tag{37}$$

where $\dot{Q}_{opt}$ and $\dot{Q}_{100\%}$ are, respectively, the condenser capacity of the optimised and the present design, while w_{opt} and $w_{100\%}$ are respectively the condenser weight of the optimised design and the present design. It is an interesting concept to reduce the metal weight (i.e. cost reduction to the manufacturer) instead of the refrigerant volume.

For the optimum condenser design, $f_o > 1$ is desired for better capacity per unit weight of the condenser. To optimise the condenser, the parameters including the wire pitch and diameter, and tube pitch and diameter were varied while maintaining the width and height of the condenser at current values. The optimisation process was carried out using the refrigerant condensing temperature of 40 °C and mass flux of 110 kg/m^2 s. The simulation results are shown in Figs. 10–13.

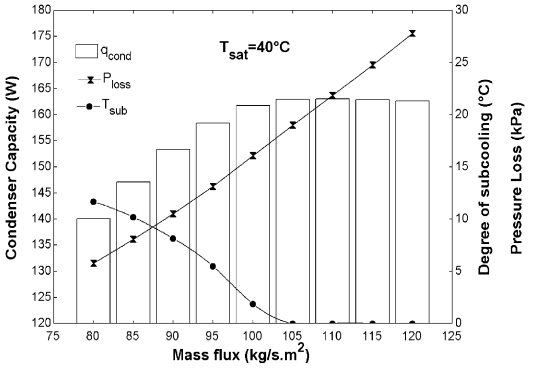

Fig. 8. Simulated condenser capacity, pressure loss and degree of sub-cooling for different mass fluxes for the W&T condenser.

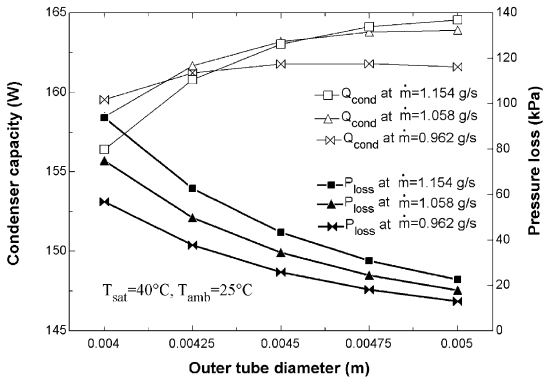

Fig. 9. Effect of mass flow rate and tube diameter on W&T condenser capacity and pressure loss.

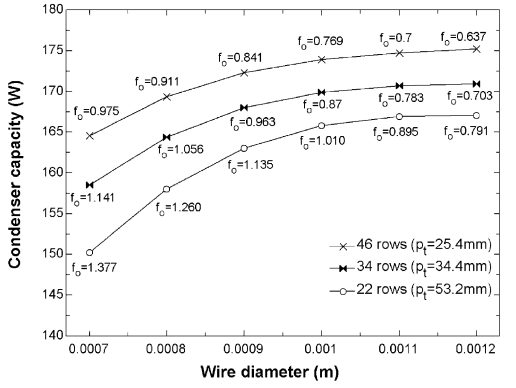

Fig. 10. Effect of tube pitch and wire diameter on condenser capacity.

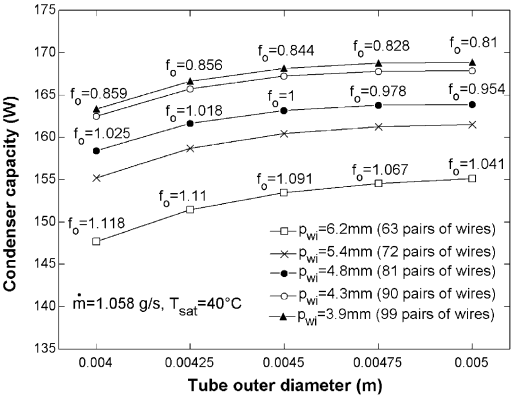

Fig. 11. Effect of wire pitch and tube outer diameter on condenser capacity.

The condenser capacity increases with increasing wire diameter as well as number of rows due to increased heat transfer area as shown in Fig. 10. However, the optimisation factor, f_o decreases with increasing wire diameter and number of rows, indicating a reduction in condenser capacity per unit weight over current condenser design. The largest f_o value is achieved with the minimum wire diameter of 0.007 m and tube pitch of 0.0532 m (22 rows) where the condenser capacity is 150 W (8% less than the current condenser design).

Alternatively, the wire pitch and tube diameter can be altered for optimisation purposes. Generally, condenser capacity is maximised with increasing tube diameter and wire density (Fig. 11). However, the effect is less than 1% when the wire pitch, $p$wi is reduced beyond 4.3 mm (90 pairs), or the diameter is increased beyond 0.045 m.

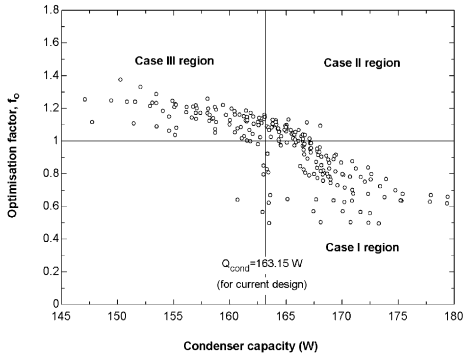

Fig. 12. Plot of the optimisation factor versus the condenser capacity.

Optimisation factor (f_o) decreases with increasing tube diameter or wire density, indicating that the condenser capacity gain is relatively small compared with the corresponding increase in condenser weight. As the wire pitch p_{wi} approaches zero, the condenser behaves much like a double array of vertical wires. In this condition, the thermal behaviour of the external side is similar to that of a constant-temperature flat plate. The gain in fins area is offset by the fact that heat transfer from the internal side is completely inhibited. The resulting Nusselt number is given by heat transfer correlation for vertical plate. For laminar flow, the average Nusselt Number applied to each surface can be approximated as [11]:

$$\overline{\mathrm{Nu}} = 0.68 + 0.67\left[\mathrm{Ra}.\left[1+\left(\frac{0.492}{\mathrm{Pr}}\right)^{9/16}\right]^{-16/9}\right]^{1/4} \quad (38)$$

where the Rayleigh Number, Ra is as given in Eq. (12b).

On the other hand, as p_{wi} becomes very large, the geometry becomes a vertical array of horizontal tubes where the Nusselt number is given by [23] as:

$$\mathrm{Nu_H} = 0.66 \times \mathrm{Ra}_{\mathrm{d_{t,o}}}^{0.25} \quad (39)$$

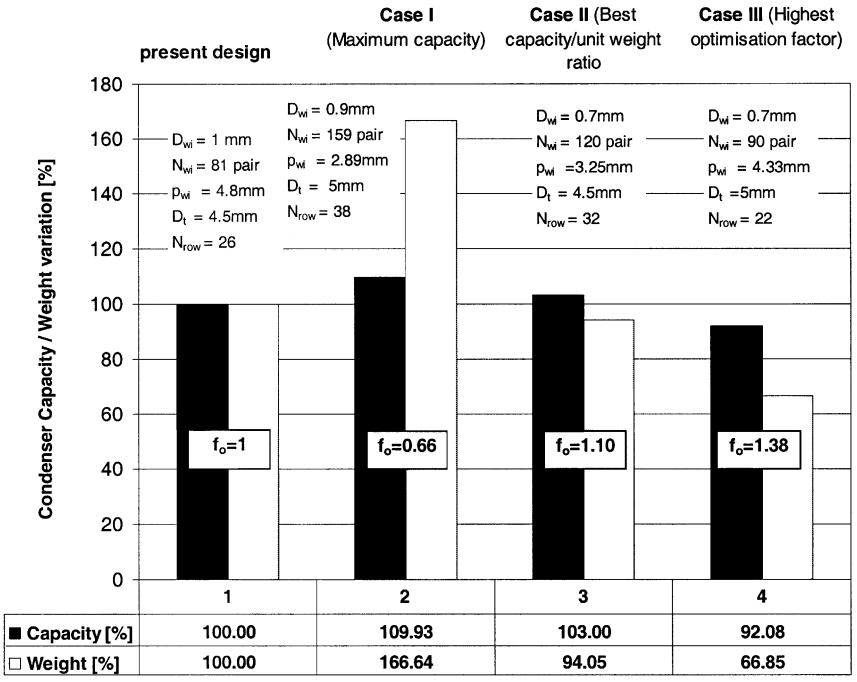

Fig. 13. Comparison of the present design with the optimised designs.

Table 3
Geometric parameters of current and optimised designs

	Present design	Case I (maximum capacity)	Case II (best capacity/ unit weight ratio)	Case III (Highest f_o)
Tube outer diameter, $d_{t,o}$ (mm)	4.5	5	4.5	5
Tube pitch, p_t (mm)	45	30.8	36.6	53.2
Number of rows	26	38	32	22
Wire diameter, d_{wi} (mm)	1	0.9	0.7	0.7
Wire pitch, p_{wi} (mm)	4.8	2.89	3.25	4.33
Number of wires (pairs)	81	159	120	90

These are the two limiting cases for the wire-and-tube geometry, and the corresponding equations [Eqs. (38) and (39)] provide the upper and lower limits for the Nusselt number.

8.2. Outcome of the optimisation process

The optimisation process uses a combination of wire density, wire diameter, tube diameter and tube pitch. Over 1000 simulations were run by varying these parameters to obtain the most efficient use of material per unit of heat transfer area. The simulated condenser capacities are plotted against the optimisation factors in Fig. 12. Generally, the optimisation factor, f_o is higher for smaller condenser capacity. It deteriorates with higher condenser capacities due to increasing weight of the condenser. Three significant outcomes were extracted from the simulation results and are shown in Fig. 13.

8.2.1. Case I: maximum capacity

The maximum capacity is achieved with the maximum number of wires and number of rows with a tube diameter of 0.9 mm (Fig. 13). However, not all values of the condenser parameters were tested due to the constraints imposed on the tube and wire pitch and diameter for the Tagliafico and Tanda [3] convective heat transfer correlation. Nevertheless, it is clear that the effort for maximum capacity is redundant due to significantly larger increase in the material weight as indicated by the reduced optimisation factor in **Case I** region in Fig. 12. Therefore, a bigger condenser (with additional rows) needs to be used to achieve larger condenser capacity.

8.3. Case II: best capacity/unit weight ratio

The optimised design is the one which yields increased condenser capacity as well as reduced condenser weight over the current design, as represented by the data in the **Case II** region in Fig. 12. Generally, increasing the fins diameter and tube and fin density can increase the capacity, however, this also increases the weight. In this study, an optimised design is obtained using a smaller wire diameter, larger fins and tube density (see Table 3). This results in 3% increase in capacity and 6% reduction in weight (Fig. 12). Essentially, this is the best condenser design. However, the improvement is not huge, indicating that the current condenser may be near optimum to some extent.

8.3.1. Case III: highest optimisation factor

Most of the simulation results produce relatively close but smaller condenser capacity (compared with the current model), with very significant reduction in the weight as shown in the **Case III** region. The highest optimisation factor of 1.38 is obtainable using the design parameters shown in Table 3. This design yields an 8% reduction in the condenser capacity but a very considerable weight saving of 34%. In fact, if the capacity reduction is acceptable in some applications, the design (Case III) using the optimised parameters in Table 3 is the most economical.

9. Conclusions

The modeling results show that the outer heat transfer resistance contributes to about 80 and 83–95% of the total heat transfer for single and two-phase flow respectively. The dominant heat transfer mode for the W&T condenser is by convection, which contributes up to 65% of the total heat transfer. The optimisation process uncovers two improved designs. The condenser design with the best capacity/weight ratio has 3% gains while 6% weight reduction. On the other hand, the design with the highest optimisation factor, f_o, though having 8% reduction in capacity, requires only 66% of the current condenser weight. Future investigations may include the design and optimisation of fan forced-convective condensers with different geometries and additional design factors such as air velocity, angle of attack and influence of mixed convection regime [1,2].

Acknowledgements

The authors are thankful to Fisher & Paykel Ltd for sponsoring the project. In particular, special thanks to Messrs Ian McGill and David Thomas (of F&P) for their invaluable input and stimulating discussions during the project.

References

[1] Hoke JL, Clausing AM, Swofford TD. An experimental investigation of convective heat transfer from wire-on-tube heat exchangers. Journal of Heat Transfer 1997;119:348–56.
[2] Lee T-H, Lee J-YYJ-S. Determination of airside heat transfer coefficient on wire-on-tube type heat exchanger. International Journal of Heat and Mass Transfer 2001;44: 1767–76.
[3] Tagliafico L, Tanda G. Radiation and natural convection heat transfer from wire-and-tube heat exchangers in refrigeration appliances. International Journal of Refrigeration 1997;20(7):461–9.
[4] Admiraal DM, Bullard CW, Experimental validation of heat exchanger models for refrigerator/freezers. ASHRAE Transactions: Research, 1994.
[5] Bansal PK, Purkayastha B. An NTU-e model for alternative refrigerants. International Journal of refrigeration 1997;21(5):381–97.
[6] Bansal PK, Wich J, Chen T, Browne M. Design and modeling of new egg-crate-type forced flow evaporators in domestic refrigerators. ASHRAE Transactions 2001;107(2).
[7] Judge J, Radermacher R. A heat exchanger model for mixtures and pure refrigerant cycle simulations. International Journal of Refrigeration 1997;20(4):244–55.
[8] Pettit NBOL, Willatzen M, Ploug-Sorensen M. A general dynamic simulation model for evaporators and condensers in refrigeration. Part II: simulation and control of an evaporator. International Journal of Refrigeration 1998;21(5): 404–14.
[9] Reeves RN, Bullard CW, Crawford RR. Measurement of refrigerator component performance. ASHRAE Transactions: Symposia 1994;20(1):1335–42.
[10] NIST, Thermodynamic and transport properties of refrigerants and refrigerant mixtures—REFPROP. 6th ed. 1998.
[11] Mills AF. Basic heat and mass transfer. 2nd ed. Upper Saddler River, (NJ): Prentice Hall; 1999.
[12] Breber G, Palen JW, Taborek J. Prediction of horizontal tubeside condensation of pure components using flow regime criteria. Journal of Heat Transfer 1980;102:471–6.
[13] Cavillini A, Zecchin R. High velocity condensation of R-11 vapors inside vertical tubes. Heat transfer in refrigeration. International Institute of Refrigeration 1971:385–96.
[14] Corberan JM, Melon MG. Modelling of plate finned tube evaporators and condensers working with R134a. International Journal of Refrigeration 1997;21(4):273–84.
[15] Boissieux X, Heikal MR, Johns RA. Two-phase heat transfer coefficients of three HFC refrigerants inside a horizontal smooth tube, part II: condensation. International Journal of Refrigeration 1999 2000;23:345–52.
[16] Cavallini A, Col DD, Doretti L. Condensation of R-22 and R407c inside horizontal tube. In: 20th International Congress of Refrigeration, IIR/IIF, Sydney, 1999.
[17] Kakac S, Liu H. Heat exchangers selection, rating and thermal design. New York: CRC Press; 1998.
[18] Jaster H, Kosky PG. Condensation heat transfer in a mixed flow regime. International Journal of Heat and Mass Transfer 1976;19:95–9.
[19] Mueller AC. Condensers—heat transfer. In: Schlunder EU, editor. Heat exchange design handbook [section 3.4.6]. New York: Hemisphere Publishing Corporation; 1983.
[20] Lockhart Rw, Martinelli RC. Proposed correlation data for isothermal two phase, two-component flow in pipes. Chemical Engineering Proceedings 1949;45:39–48.
[21] Chin TC. Experimental and numerical study of the wire-and-tube and hotwall condensers for domestic refrigerators. ME thesis, The Department of Mechanical Engineering, The University of Auckland, New Zealand, 2001.
[22] Bansal PK, Wich T. Optimisation of egg-crate type evaporators in domestic refrigerators. Applied Thermal Engineering 2001;21:751–70.
[23] Tanda G, Tagliafico L. Free convection heat transfer from wire-and-tube heat exchanger. Journal of Heat Transfer 1997;119(May):370–2.